International Journal of Cast Metals Research

ISSN: 1364-0461 (Print) 1743-1336 (Online) Journal homepage: http://www.tandfonline.com/loi/ycmr20

Macro and microstructural characterisation of high Si cast steels – Study of microsegregation patterns

Nicolás E. Tenaglia, Roberto E. Boeri, Alejandro D. Basso & Juan M. Massone

To cite this article: Nicolás E. Tenaglia, Roberto E. Boeri, Alejandro D. Basso & Juan M. Massone (2016): Macro and microstructural characterisation of high Si cast steels – Study of microsegregation patterns, International Journal of Cast Metals Research, DOI: 10.1080/13640461.2016.1258515

To link to this article: http://dx.doi.org/10.1080/13640461.2016.1258515

Published online: 23 Nov 2016.

INTERNATIONAL JOURNAL OF CAST METALS RESEARCH, 2016
http://dx.doi.org/10.1080/13640461.2016.1258515

Taylor & Francis
Taylor & Francis Group

Macro and microstructural characterisation of high Si cast steels – Study of microsegregation patterns

Nicolás E. Tenaglia, Roberto E. Boeri, Alejandro D. Basso and Juan M. Massone

Department of Metallurgy, INTEMA – CONICET, University of Mar del Plata, Mar del Plata, Argentina

ABSTRACT

In this study the as-cast macro and microstructures of medium C – high Si cast steels of three different levels of alloying are characterised. The application of a colour-etching reagent sensitive to Si segregation effectively revealed the solidification macrostructure, showing that the patterns of macrostructure and microsegregation are governed by the initial precipitation of δ-ferrite dendrites. A study of microsegregation carried out using advanced EDS techniques showed that, for the studied chemical compositions, Si, Mn, Cr, Ni, Mo and Al tend to concentrate at the last liquid to solidify. Accordingly, effective partition coefficients of values below unity were calculated for all alloying elements tested. It was verified that the minimum local Si contents measured on the steels investigated were greater than 1.7%, value above the minimum value (1.5%) necessary to obtain carbide-free bainite after austempering.

ARTICLE HISTORY
Received 4 August 2016
Accepted 31 October 2016

KEYWORDS
Cast steels; high silicon; microsegregation; solidification; peritectic

1. Introduction

This study is part of a project that aims at developing high Si cast steels of chemical compositions appropriate to be austempered, obtaining carbide-free bainitic structures. This kind of steels is of particular interest because the high content of Si retards the carbide precipitation during the bainite transformation, obtaining a fine mixture of ferrite and retained austenite that presents excellent mechanical properties and toughness. Most studies reported in the literature related to carbide-free bainitic steels are centred on the determination of their mechanical and wear properties depending on the chemical composition and heat treatment variables.[1–4] However, most of these studies were conducted on steels that have previously undergone extensive thermomechanical treatments, such as homogenisation heat treatment, hot rolling or forging, which significantly affected the segregation patterns caused during solidification.

Many steel parts applicable to the automotive, mining or oil industries can be obtained through the melting and casting technique (crankshafts, camshafts, pump bodies, suspension parts, etc.), and these pieces have different geometries and varying thicknesses. It is widely recognised that the mechanical properties of castings differ from those obtained on rolled or forged parts of the same chemical composition; therefore, in order to encourage the industrial application of these steels in cast parts, it is of great interest to study the solidification process, chemical segregation and the resulting mechanical properties after austempering.

The objective of this work is to characterise the solidification macro and microstructure of high Si cast steels with three different chemical compositions. Particular interest is given to the microsegregation of alloy elements, as this noticeably affects the microstructure after austempering.

2. Experimental procedure

2.1. Material

Three different steels were designed. Steel 1 corresponds to the composition limits of ASTM 9200 series (Silicon steels); Steel 2 is similar to Steel 1 but in this melt Cr, Ni and Mo were added with the intention of increasing its hardenability; Steel 3 is similar to Steel 2 but it also includes Al and Co, as these elements have been reported to accelerate the rate of transformation of austenite at the austempering temperature range.[5]

The material was prepared in an industrial foundry using a medium frequency induction furnace of 80 kg capacity. Selected steel scrap and ferroalloys were used as raw materials. The melts were poured in Keel-block-shaped sand moulds (ASTM A-703). The chemical composition was determined using a Baird DV6 spectrometer. Si content was measured by gravimetry and C by combustion.

CONTACT Nicolás E. Tenaglia ntenaglia@fi.mdp.edu.ar

Table 1. Chemical composition of steels (wt.%).

	C	Si	Mn	Cr	Ni	Mo	Al	Co	S	P
Steel 1	0.45	2.13	0.60						0.0076	0.017
Steel 2	0.40	2.06	0.59	0.52	0.49	0.53			0.0048	0.010
Steel 3	0.43	2.06	0.58	0.59	0.56	0.53	0.61	0.21	0.0095	0.022

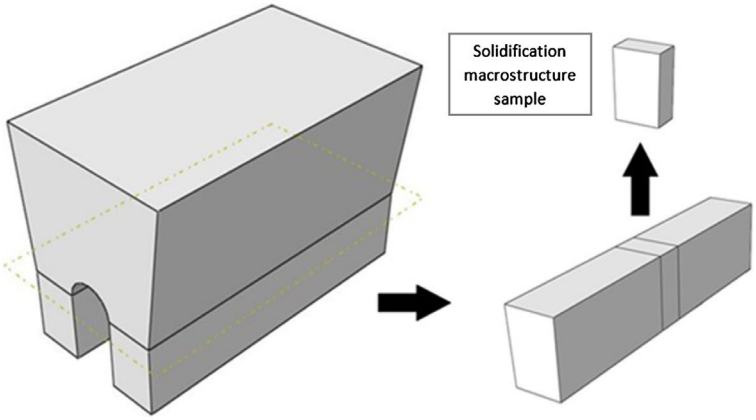

Figure 1. Solidification macrostructure samples.

The resulting chemical composition of steels is shown in Table 1.

2.2. Macro and microstructural characterisation

The metallographic characterisation of the as-cast structures was performed using conventional methods of cutting and polishing. The polished surfaces were etched with several reagents, as nital (2%), Oberhoffer and also colour etching. Colour etching consists in the application of a special reagent to the polished surfaces with the aim of revealing the segregation pattern generated during solidification. The etchant consists of 10 g NaOH, 40 g KOH, 10 g picric acid and 50 ml of distilled water. It must be applied while boiling and with particular care, as it is toxic. Its use requires considerable expertise, particularly at selecting the etching time according to the chemical composition of the alloy. Etching produces the deposition of thin oxide films (about 0.04 and 0.5 µm) over the specimen surface. The thickness of the films depends on Si concentration and because of the light interference phenomenon, different thicknesses produce different colours, allowing the identification of the Si segregation pattern. This technique is commonly used in cast iron to reveal last to freeze (LFT) and first to freeze (FTF) zones.[6]

The solidification macrostructure was evaluated on samples cut from the blocks as shown in Figure 1. After etching with nital, several optical micrographies were taken along the surface. Then, the metallographies were assembled to represent a greater area when necessary. After that, the samples were re-polished and Oberhoffer regent was applied to reveal the dendritic structure.

The dendrite secondary arm spacing was measured on colour etched samples, where dendrite arms were readily revealed. Small samples were extracted from level 2 of keel blocks (Figure 2), this is because colour etching produces better results on small pieces. Image analysis software was used to carry out the measurement, which was done along the columnar-grain zone, because in that zone it was possible to observe large dendrites and the measurement resulted more reliable.

The as-cast microstructure was characterised in level 2 samples (Figure 2). The samples were polished and etched with nital 2%.

2.3. Segregation of alloy elements

The quantification of the microsegregation of the alloy elements was made by the combined use of colour etching and EDS. First, colour etching was applied on the surfaces of three as-cast steels, with the objective of revealing first to freeze (FTF) and last to freeze (LTF) zones. Then, micro-hardness indentations were used to mark some FTF and LTF areas. Later, the surfaces were re-polished to remove the oxide layers deposited after colour etching but not the hardness indentation marks, and then analysed by EDS. Samples were taken from level 2 of the keel blocks (Figure 2). Measurements were carried out on a Carl Zeiss Sigma EDS operating at 15 kV and using Silicon Drift Detector, providing an advanced microanalysis.

Chemical composition of about 20 FTF and 20 LTF zones was measured for each steel, quantifying mass percentage of Si, Mn, Cr, Ni, Mo and Al, when appropriate. The quantification of Co was not satisfactory; therefore it was not included in the results. The degree of microsegregation was characterised by the calculation of the effective partition coefficient (K_{ef}) for each alloy element in three steels according to Equation (1), where Cs is the concentration at the location of the first solid phase

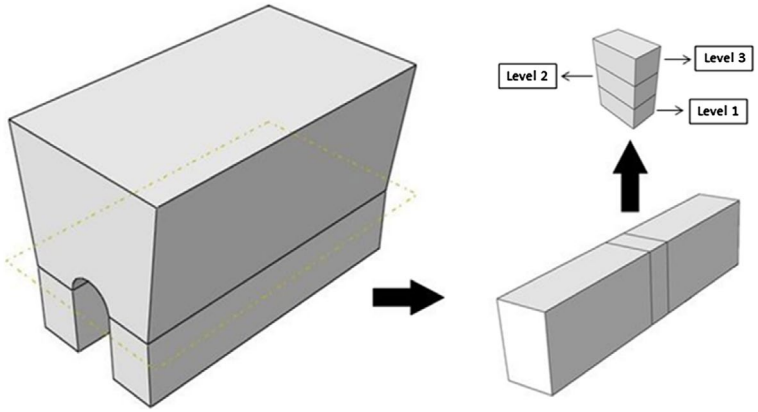

Figure 2. Samples used to measure dendrite arm spacing and to reveal solidification microstructure.

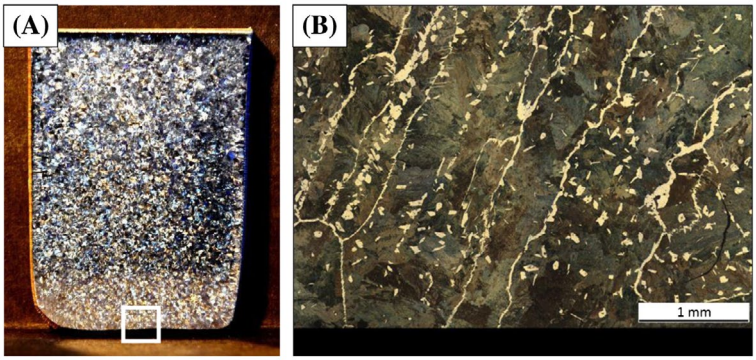

Figure 3. Steel 1 solidification macrostructure observed by naked eye (A) and by optical microscope (B).

formed, and Co is the nominal/average concentration. In this work, Cs was determined as the concentration value measured in FTF zones, while Co is the average concentration of the studied area.

$$k_{ef} = C_s/C_0 \quad (1)$$

3. Results and discussion

3.1. Solidification macrostructure

Figure 3 shows the solidification macrostructure of steel 1 revealed by nital etching. Figure 3(A) corresponds to the sample observed by naked eye and Figure 3(B) is an enlargement of the square area pointed in Figure 3(A), observed by optical microscopy. The observation of the sample by naked eye shows a finely grained structure, but does not allow to reveal solidification macrostructure clearly, however under the microscope the presence of very large grains were observed thanks to the precipitation of ferrite along the prior austenite grain boundaries.

Steels 2 and 3 showed much lesser ferrite at the austenite grain boundary, making it impossible to identify the extension of the grains by this method.

Figure 4 shows the application of Oberhoffer etching on the steels. This etchant reveals dendritic pattern and is usually used to reveal solidification macrostructure in continuous casting steels, among others. The time for the etching was 30 s and photos were taken with a digital camera in 'macro' mode. After that, images were edited in a conventional image software to improve the observation.

Images show, for three steels, very large dendrites, many of them reaching more than 10 mm length.

Both Nital and Oberhoffer etchings allowed to identify large grains or dendrites. Nevertheless, it was apparent that the pattern of austenite grains was not coincident with the dendritic pattern. Therefore, it was decided to apply colour etching to the steels to obtain more information about solidification structure. Figure 5(A), corresponding to Steel 1, shows that the colour etching technique applied is very effective in revealing a dendritic pattern. Dendrite arms, the FTF zones, appear as orange areas, while interdendritic or LTF zones are red areas surrounded by yellow, green and blue halos. In fact, it is possible to identify contraction micro-cavities in some LTF zones. In Steel 2 (Figure 5(B)), FTF zones are orange and LTF zones are green. Finally, in Steel 3 (Figure 5(C)), LTF zones appear as green areas with red halos and FTF zones appear as orange areas with red halos. The different features of the colouration obtained after the etching of the three steels, such as the different green colouration and the presence of colour fringes around the dendrites, should not be linked to any particular metallographic feature. Instead, changes in the colouring patterns can be the result of the differences in chemical composition of the steels and in the application of the

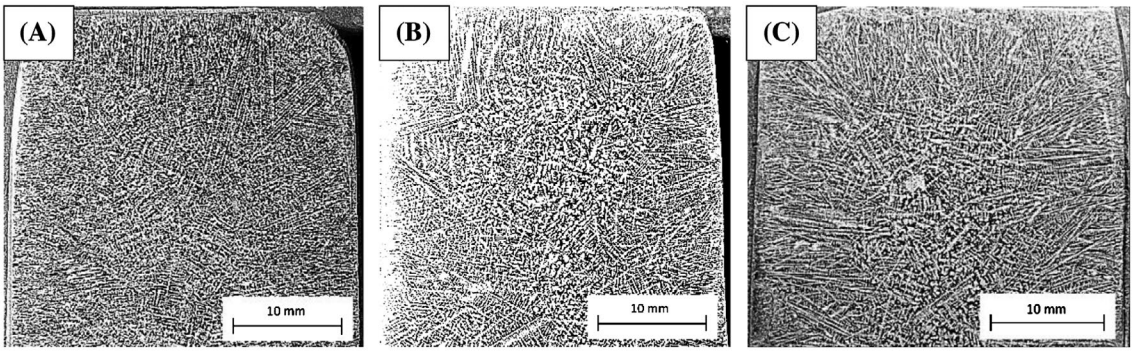

Figure 4. Oberhoffer etching. Steel 1 (A), Steel 2 (B) and Steel 3 (C).

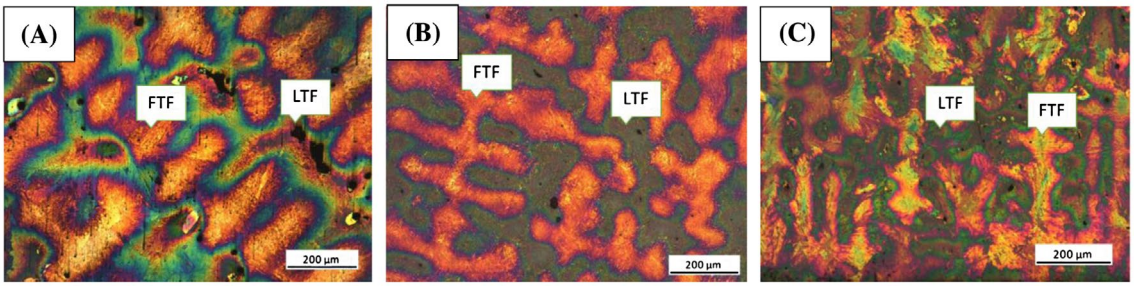

Figure 5. Identification of LFT and FTF zones. Steel 1 (A), Steel 2 (B) and Steel 3 (C).

etching. According to Rivera et.al. [6], when this colour etching reagent is applied to cast iron, green areas correspond to FTF zones and yellow/orange areas are LTF zones. However, steels presented inverted colouration, suggesting that Si shows a different behaviour in steels than in cast iron. This will be discussed below, at the time segregation coefficients are calculated.

As shown in Figure 5, the size of the dendritic patterns present in the steel samples is too large to be covered by a single metallographic field of observation. Several optical metallographies were assembled into a single picture to cover a greater surface area. This allowed to reveal the solidification macrostructure, as shown in Figures 6–8. The black area at the left side corresponds to the sample surface. The dendritic pattern already revealed by using Oberhoffer reagent is shown now in much better detail. Large dendrites of several millimetres in length are clearly revealed. It is possible to observe that steel 1, Figure 6, shows a noticeable amount of ferrite (white phase) precipitated both along what appears to be a grain boundary and as small dispersed particles. This feature is also found on steels 2 and 3, but the amount of ferrite precipitated is much smaller. The comparison of Figures 3(B) and 6 shows the utility of colour etching in revealing the underlying dendritic pattern that could not be revealed by regular etching. It is worth noting that the grain pattern highlighted by the precipitation of ferrite in steel 1 does not match the dendritic pattern, as the ferrite precipitates are not located at the areas separating neighbouring dendrites.

This phenomenon can be observed in the three steels (Figure 9(A) for Steel 1, Figure 9(B) for Steel 2, Figure 9(C) for Steel 3) where the grain boundary precipitates clearly cross dendrite arms. The location of these precipitates can be explained by analysing the solidification of this type of steel.

Figure 10 shows a pseudo-binary Fe-C diagram for 2% Si.[7] Steels having 0.40 to 0.45% C will suffer the peritectic solidification. Accordingly, the solidification will start with the nucleation and growth of δ-ferrite. After approximately 60% of the volume has transformed into δ-ferrite, the steel reaches the peritectic temperature and the peritectic reaction starts. In the peritectic reaction,[8] the melt reacts with δ-ferrite to form γ-austenite while the three phases are in contact. Austenite nucleates at the δ-ferrite/liquid interface and then grows laterally along the surface of δ-ferrite, by diffusion of solute atoms from δ to ferrite into γ-austenite through the melt. The lateral growth continues until γ-austenite covers the surface of δ-ferrite completely and separates it from the melt. The peritectic transformation begins at that point, where the γ-austenite layer surrounding δ-ferrite grows into the melt and into δ-ferrite simultaneously until the complete annihilation of δ-ferrite.

Since austenite nucleates and grows on the surface of δ-ferrite dendrites, several austenite grains can nucleate from a single δ-ferrite dendrite, and the peritectic solidification results in several grains of austenite surrounding each δ-ferrite dendrite. As the transformation advances, the different austenite grains grow and interact, defining

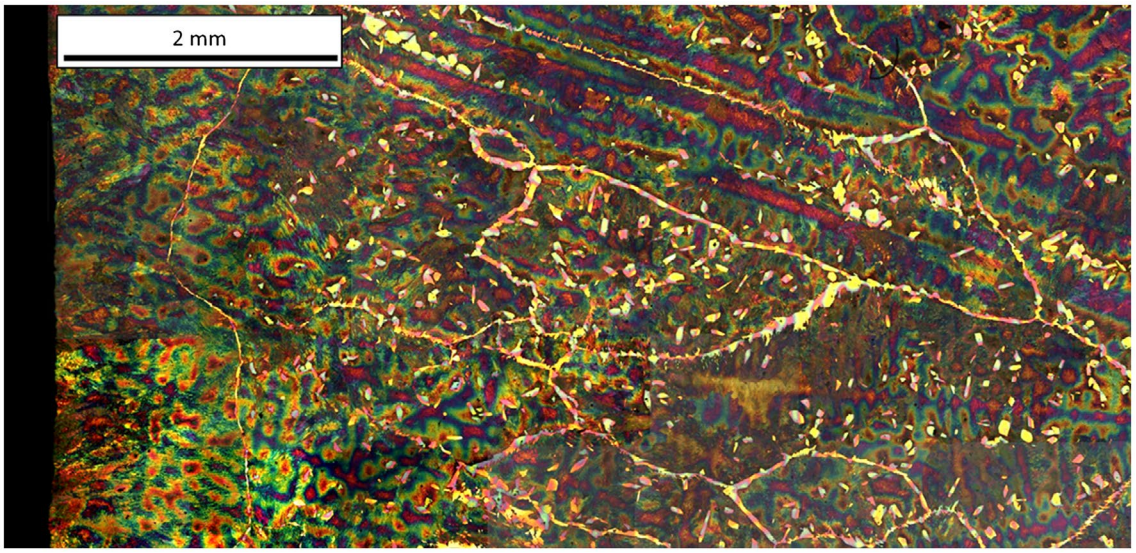

Figure 6. Steel 1 solidification macrostructure reveal by colour etching.

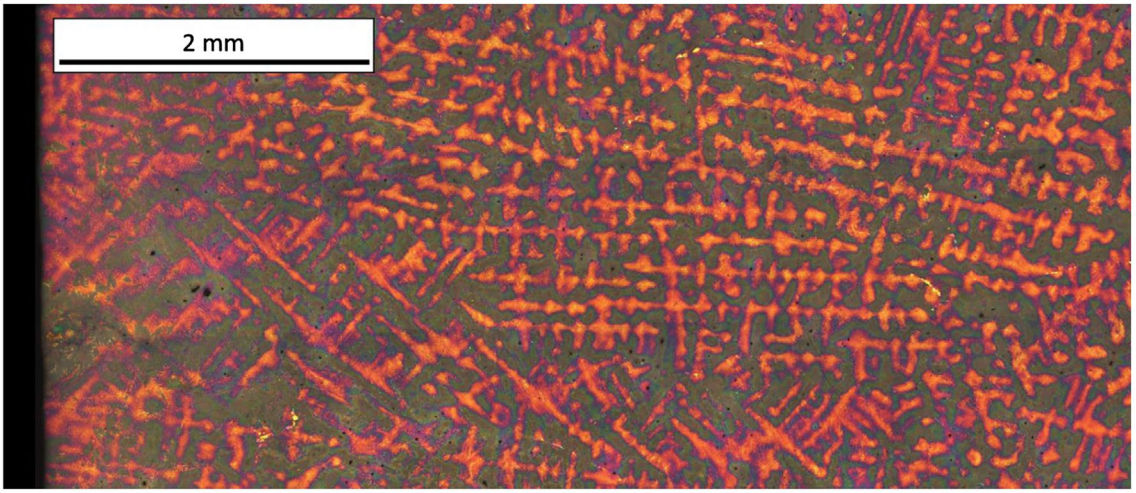

Figure 7. Steel 2 solidification macrostructure reveal by colour etching.

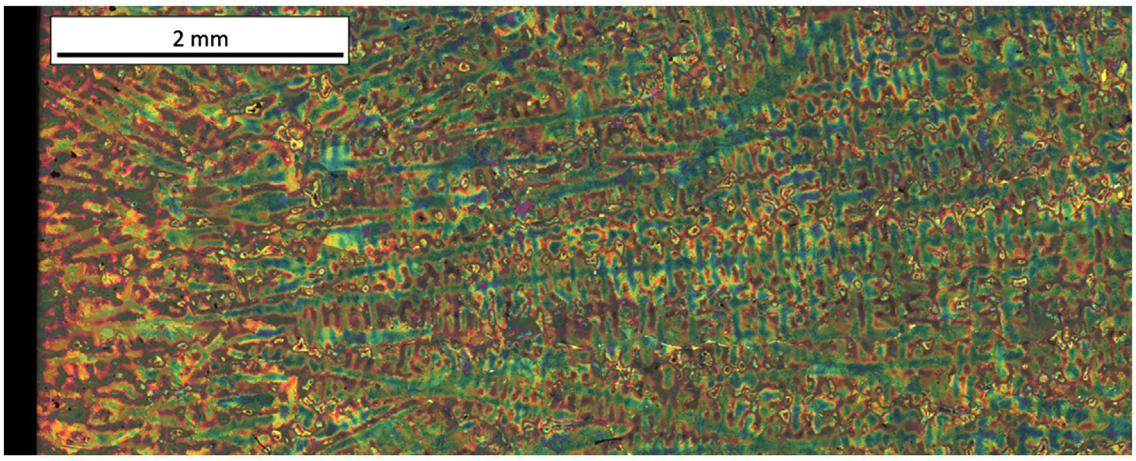

Figure 8. Steel 3 solidification macrostructure reveal by colour etching.

boundaries that cross the initial δ-ferrite dendritic pattern, as shown in Figure 9.

By revealing the dendritic pattern, colour etching also allows the measurement of secondary arm spacing. This parameter is important because, together with the effective partition coefficients, it can be used to characterise the microsegregated zones: a small secondary arm spacing will result in a more homogenous microstructure

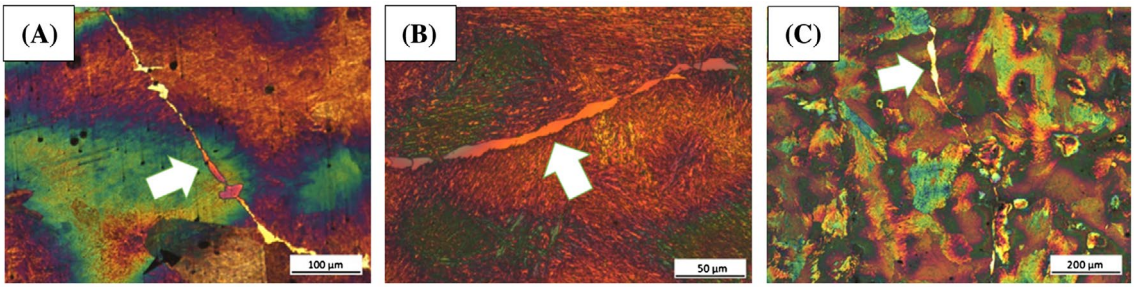

Figure 9. Grain boundaries crossing dendrites. Steel 1 (A), Steel 2 (B) and Steel 3 (C).

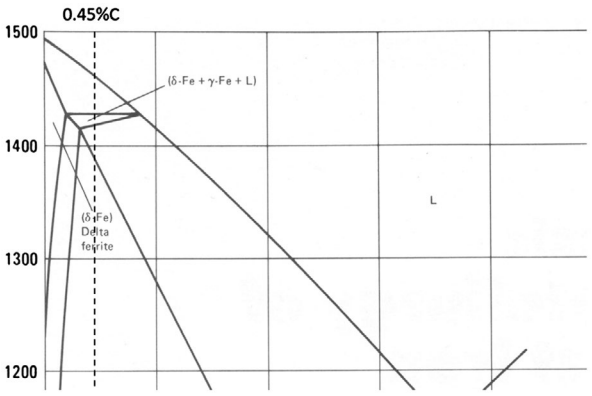

Figure 10. Portion of Fe-C equilibrium diagram for 2% Si.[7]

after heat treatments. Figure 11 shows some examples of the measurement of secondary dendrite arm spacing and Table 2 shows the results. The reported values are the minimum value measured for each steel, because in this manner non-parallel to surface dendrites are discarded. It is possible to observe that the measured values are the same for the three steels, indicating that the chemical composition has negligible influence on the dendritic arm spacing, as expected according to Cahn [9].

3.2. As-cast microstructure and hardness

Although high Si steels obtain their relevant mechanical properties after austempering, their as-cast microstructure and hardness are relevant characteristics for the processing of castings before heat treating. The microstructure of Steel 1 revealed by nital 2% etching is shown in Figure 12. At low magnification, allotriomorphic, idiomorphic and Widmanstätten ferrite can be identified

Table 2. Secondary dendrite arm spacing.

Steel 1	Steel 2	Steel 3
76 µm	79 µm	79 µm

(Figure 12(B) and (C)). At higher magnification pearlite is found to form the matrix (Figure 12(A)). Most idiomorphic ferrite precipitates (located inside the grains) show inclusions inside that may have acted as nucleation sites. Grain boundary ferrite shows two different morphologies: most are allotriomorphic (Figure 12(B)), although near the surface of the casting, Widmanstätten ferrite was also observed (Figure 12(C)), caused by the higher cooling rate imposed in that zone after solidification.

Steel 2 microstructure is bainitic in as-cast condition (Figure 13(A)) with some allotriomorphic ferrite precipitated at austenite grain boundary (Figure 13(B)). Compared to Steel 1, Steel 2 presents lesser quantity of ferrite and no Widmanstätten ferrite. This microstructure is expected because steel 2 presents a considerable quantity of Mo and this alloy element causes a retardation of the pearlitic transformation.

Finally, Steel 3 shows a bainitic microstructure (Figure 14(A)) with allotriomorphic ferrite in grain boundary (Figure 14(B)) and some idiomorphic ferrite inside grains (Figure 14(C)). As for steel 2, bainitic microstructure in steel 3 is attributed to the Mo content.

The as-cast hardness of the steels were 253 HB for Steel 1, 363 HB for Steel 2 and 368 HB for Steel 3.

3.3. Microsegregation

Figure 15(A) shows the colour etched microstructure of a sample of steel 2. Microhardness indentations have been

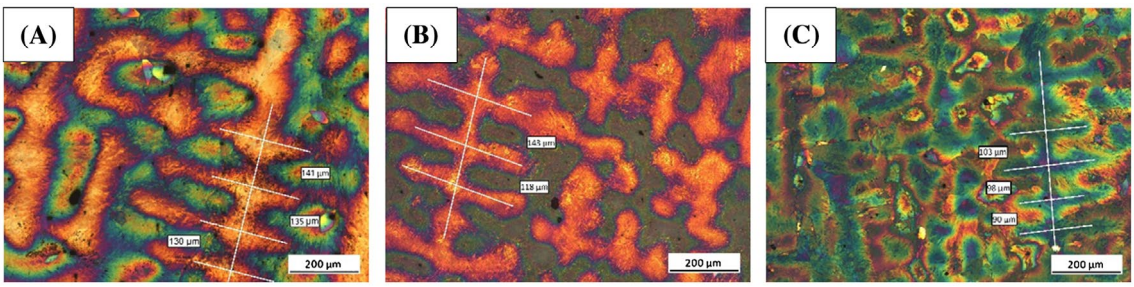

Figure 11. Secondary dendrite arm spacing measurement. Steel 1 (A), Steel 2 (B) and Steel 3 (C).

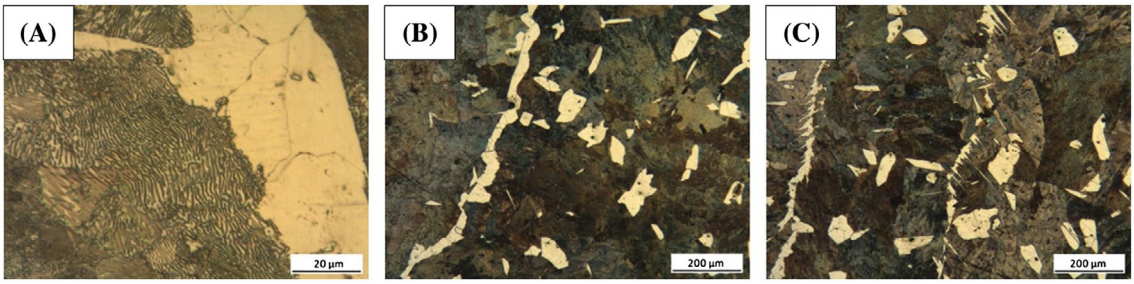

Figure 12. Steel 1. Pearlitic-Ferritic microstructure (A), Allotriomorphic ferrite (B) and Widmanstätten ferrite (C).

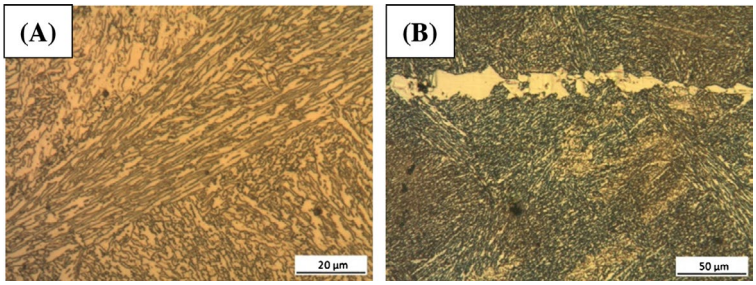

Figure 13. Steel 2. Bainitic microstructure (A) and Allotriomorphic ferrite in grain boundary (B).

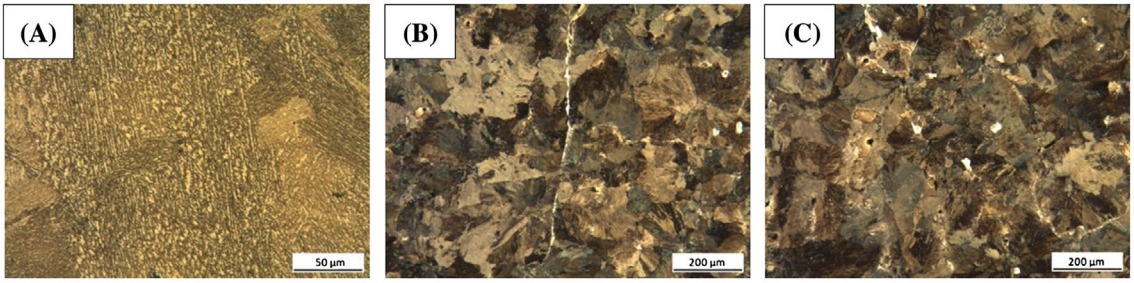

Figure 14. Steel 3. Bainitic microstructure (A), Allotriomorphic ferrite in grain boundary (B) and Idiomorphic ferrite inside grains (C).

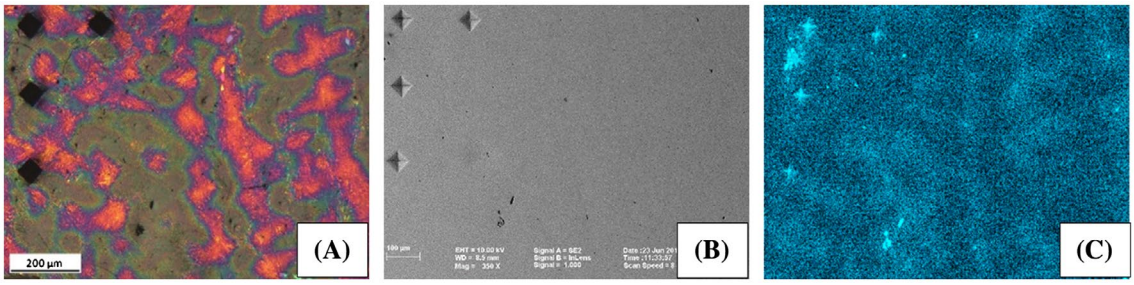

Figure 15. Steel 2. Colour etching (A), SEM image (B) and Silicon mapping (C).

made on the sample in order to keep track of the location of the dendritic patterns after repolishing. Figure 15(B) shows the same area of Figure 15(A) under the SEM after re-polishing to remove the etching products. The complete area shown in Figure 15(B), of about 1 mm^2 is scanned by the EDS. Figure 15(C) shows a Si mapping of the area of Steel 2 under analysis (note the position of indentations), where brighter zones correspond to

Table 3. Chemical composition measured by EDS and analytically (wt.%).

		Si	Mn	Cr	Ni	Mo	Al
EDS	Steel 1	2.2	0.7				
	Steel 2	2.1	0.7	0.5	0.5	0.5	
	Steel 3	2.3	0.7	0.6	0.5	0.5	0.6
Analytical	Steel 1	2.13	0.60				
	Steel 2	2.06	0.59	0.52	0.49	0.53	
	Steel 3	2.06	0.58	0.59	0.56	0.53	0.61

Table 4. Minimum and maximum values and partition coefficient.

		Si	Mn	Cr	Ni	Mo	Al
Steel 1	Minimum (wt.%)	1.7	0.4				
	Maximum (wt.%)	3.2	1.3				
	K_{ef}	0.77	0.57				
Steel 2	Minimum (wt.%)	1.7	0.4	0.3	0.3	0.2	
	Maximum (wt.%)	3.1	1.3	0.9	0.9	1.6	
	K_{ef}	0.81	0.57	0.60	0.60	0.40	
Steel 3	Minimum (wt.%)	1.9	0.4	0.4	0.3	0.2	0.3
	Maximum (wt.%)	2.7	0.9	0.8	1.0	1.1	0.7
	K_{ef}	0.83	0.57	0.66	0.60	0.40	0.50

higher Si concentration. Note that brighter areas match with LTF zones as revealed by colour etching, while darkener areas match with FTF zones. Therefore, EDS analysis verifies that the colour etching technique applied is sensitive to Si concentration, in coincidence with previous reports for cast iron.[6]

Table 3 shows the average chemical composition of the three steels measured by EDS and a comparison with the analytical results listed on Table 1. The global chemical composition is an average of every point in the studied area, which was divided in 1024 × 1024 pixels. The EDS readings are in reasonably good agreement with the analytical results.

Point EDS analysis was carried out at FTF and LTF areas. Table 4 lists the minimum and maximum concentration values measured at the FTF and LTF, respectively, calculated as the average of the three minimum and maximum readings. The quantitative results verify that all tested elements accumulate at LTF zones, while FTF zones are alloy element depleted zones. Therefore, the initial effective partition coefficient of an alloying element can be approximated as the concentration of the FTF solid over the average concentration. This assumes that the microsegregation generated at the time of the start of solidification suffers negligible homogenisation during the subsequent cooling to room temperature. This is a reasonable assumption for substitutional alloying elements, such as those investigated in this case. Calculated effective partition coefficients for each element and steel are listed on Table 4. Note that these partition coefficients correspond to the partition between δ-ferrite and the liquid melt. Taking in account the experimental error of EDS, it can be concluded that the partition coefficients for all elements tested are the same in the three steels.

The comparison of the calculated partition coefficients with equilibrium partition coefficients reported in the literature for Fe-X binary systems, Table 5, shows that the values quoted for Si are similar, however the calculated coefficients for Mn, Cr, Ni and Al are different from those reported by Battle [10] and Ueshima [11]. This discrepancy is understandable because the equilibrium coefficients referenced were calculated for binary systems, while the experimental coefficients were measured on multi-component alloys. The microsegregation of a particular element may be influenced by the concentration of other elements.

Table 5. Comparison of calculated partition coefficients with those reported in literature.

	This work	Battle [10]	Ueshima [11]
Si	0.77–0.83	0.83	0.77
Mn	0.57	0.9	0.76
Cr	0.60–0.66	0.95	
Ni	0.60	0.83	
Al	0.50	0.92	

Minimum and maximum values of solute concentration, together with the secondary dendrite arm spacing, constitute a good characterisation of the intensity and extent of microsegregation in this type of steel.

The microsegregation found in this type of steels indicates that future heat treatments, particularly austempering treatments to obtain carbide-free bainite, will see the solid state reactions to proceed at a different rate in LTF zones than in FTF, since the greater concentration of alloying elements at the LTF will delay the diffusional transformations of austenite, increasing local hardenability and austemperability. Therefore, the bainitic transformation will begin at FTF zones and then extend to LTF zones. Proper austempering heat treatment cycles should account for the heterogeneity present in the metal matrix. In addition, the microsegregation study has shown that the proposed chemical compositions show minimum concentrations of Si in excess of 1.5%, which is regarded as the minimum amount of Si needed to produce carbide-free bainitic steels.[2]

Conclusions

The study of the solidification of three high Silicon steels showed that:

- The application of a colour etching reagent sensitive to Si segregation on the medium C – high Si steels studied effectively revealed their solidification macrostructure.
- The patterns of macrostructure and microsegregation are governed by the initial precipitation of δ-ferrite dendrites.
- As-cast microstructures for Si alloyed Steel 1 (corresponding to AISI 9200 series) is mainly pearlitic, presenting α-ferrite in different morphologies (allotriomorphic, idiomorphic and Widmanstätten). On the other hand, steels 2 and 3, alloyed with Si, Mo, Ni and Cr showed bainitic microstructure as cast as a result of the presence of Mo in the alloy.
- The presence of large austenite grains formed after the peritectic transformation was evident thanks to the precipitation of proeutectic ferrite along its grain boundary.

- The study of microsegregation carried out using advanced EDS techniques showed that, for the studied chemical compositions, Si, Mn, Cr, Ni, Mo and Al tend to concentrate at the last liquid to solidify. Accordingly, effective partition coefficients were below unity.
- The minimum local Si content measured on the steels investigated was 1.7%, value above the limit value of 1.5% necessary to obtain carbide-free bainite after austempering.

Disclosure statement

No potential conflict of interest was reported by the authors.

Funding

This work was supported by ANPCyT and MINCyT of Argentine and Fondo para la Investigacion Cientifica y Tecnologica [grant number PICT 12-1146].

ORCID

Nicolás E. Tenaglia http://orcid.org/0000-0001-6372-8881
Roberto E. Boeri http://orcid.org/0000-0001-7083-579X
Juan M. Massone http://orcid.org/0000-0003-1287-1463

References

[1] Caballero FG, Chao J, García-Mateo C, et al. Toughness of advanced high strength bainitic steels. Mater Sci Forum. 2010;638–642:118–123.
[2] Garcia-Mateo C, Caballero FG, Sourmail T, et al. Tensile behaviour of a nanocrystalline bainitic steel containing 3 wt% silicon. Mater Sci Eng A. 2012;549:185–192.
[3] Morales-Rivas L, Wie-Hung Y, Bo-Ming H, et al. Tensile response of two nanoscale bainite composite-like structures. JOM – J Min Met Mat S. 2015;67:2223–2235.
[4] Peet MJ, Hill P, Rawson M, et al. Fatigue of extremely fine bainite. Mater Sci Technol. 2011;27:119–123.
[5] Garcia-Mateo C, Caballero FG, Bhadeshia HKDH. Acceleration of low-temperature bainite. ISIJ Int. 2003;43:1821–1825.
[6] Rivera G, Boeri R, Sikora J. Revealing the solidification structure of nodular iron. Int J Cast Met Res. 1995;8:1–5.
[7] Cubberly WH. Metals handbook. 9th ed. Vol. 1, Properties and selection: iron and steels. Russell Township (OH): American Society for Metals; 1978.
[8] Stefanescu DM. Microstructure evolution during the solidification of steel. ISIJ Int. 2006;46:786–794.
[9] Cahn RW, Haasen P. Physical metallurgy. Vol. 1. Amsterdam: Elsevier Science; 1996.
[10] Battle TP, Pehlke RD. Equilibrium partition coefficients in iron-based alloys. Metall Trans B. 1989;20:149–160.
[11] Ueshima Y, Mizoguchi S, Matsumiya T, et al. Analysis of solute distribution in dendrites of carbon steel with δ/γ transformation during solidification. Metall Trans B. 1986;17:845–859.